Interpretation of Scanning Tunneling Quasiparticle Interference and Impurity States in Cuprates

A. Kreisel,[1,4] Peayush Choubey,[1] T. Berlijn,[2] W. Ku,[3] B. M. Andersen,[4] and P. J. Hirschfeld[1]

[1]*Department of Physics, University of Florida, Gainesville, Florida 32611, USA*

[2]*Center for Nanophase Materials Sciences and Computer Science and Mathematics Division, Oak Ridge National Laboratory, Oak Ridge, Tennessee 37831, USA*

[3]*Condensed Matter Physics and Materials Science Department, Brookhaven National Laboratory, Upton, New York 11973, USA*

[4]*Niels Bohr Institute, University of Copenhagen, DK-2100 Copenhagen, Denmark*

(Received 6 July 2014; published 27 May 2015)

We apply a recently developed method combining first principles based Wannier functions with solutions to the Bogoliubov–de Gennes equations to the problem of interpreting STM data in cuprate superconductors. We show that the observed images of Zn on the surface of $Bi_2Sr_2CaCu_2O_8$ can only be understood by accounting for the tails of the Cu Wannier functions, which include significant weight on apical O sites in neighboring unit cells. This calculation thus puts earlier crude "filter" theories on a microscopic foundation and solves a long-standing puzzle. We then study quasiparticle interference phenomena induced by out-of-plane weak potential scatterers, and show how patterns long observed in cuprates can be understood in terms of the interference of Wannier functions above the surface. Our results show excellent agreement with experiment and enable a better understanding of novel phenomena in the cuprates via STM imaging.

DOI: 10.1103/PhysRevLett.114.217002 PACS numbers: 74.20.-z, 74.62.En, 74.70.Xa, 74.81.-g

Scanning tunneling microscopy (STM) methods were applied to cuprates relatively early on, but dramatic improvements in energy and spatial resolution led to a new set of classic discoveries in the early part of the last decade, giving for the first time a truly local picture of the superconducting and pseudogap states at low temperatures [1,2]. These measurements revealed gaps that were much more inhomogeneous than had previously been anticipated [3–6], exhibited localized impurity resonant states [7,8], and gave important clues to the nature of competing order [9–13]. More recently, STM has again been at the forefront of studies of inhomogeneities, this time as a real space probe of intraunit cell charge ordering visible in the underdoped systems [14]. While a microscopic description of such atomic scale phenomena in superconductors is available in terms of the Bogolibuov–de Gennes (BdG) equations, such calculations are always performed on a lattice with sites centered on the Cu atoms, and thus do not contain intraunit cell information.

The simplest example of a problem that can arise because of the deficiencies of theory in this regard is that of the Zn impurity substituting for Cu in $Bi_2Sr_2CaCu_2O_8$ (BSCCO), a cuprate material which cleaves well in vacuum, leaving atomically smooth surfaces ideal for STM. The observation of a spectacularly sharp impurity resonance at the impurity site [7,8,15,16] was an important local confirmation of unconventional pairing in the cuprates. The differential conductance map near the impurity exhibits a cross-shaped real-space conductance map at resonance, as expected for a pointlike potential scatterer in a *d*-wave superconductor; see Fig. 1(c) [17]. Upon closer examination, however, the pattern deviates from the expected theoretical one on the Cu square lattice in some important respects [18,19]. First, it displays a central maximum on the impurity site, unlike simple models, which have a minimum [Fig. 1(a)]. Second, the longer range intensity tails are rotated 45 degrees from the nodal directions of the *d*-wave gap, where such long quasiparticle decay lengths are expected [18]. There is still no consensus on the origin of this pattern, which has been discussed in terms of nonlocal Kondo correlations [20], postulated extended potentials [21–23], Andreev phase impurities

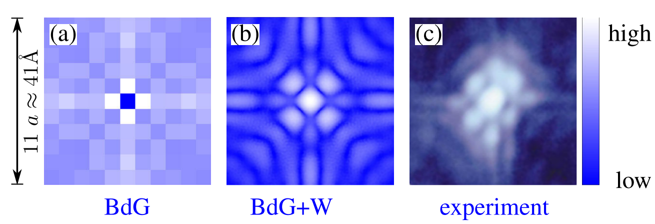

FIG. 1 (color online). (a) Resonant state real-space BdG patterns at $\Omega_0 = -3.6$ meV as obtained from conventional BdG calculations in logarithmic scale, (b) *xy* cut through continuous 3D LDOS $(x, y, z \approx 5$ Å$; \Omega_0)$ at $\Omega_0 = -3.6$ meV showing strong similarity to the measured conductance maps (c) reproduced from Ref. [8] rotated to match the orientation in (a) and (b) and cropped to 11×11 elementary cells with the impurity located at the center.

[24], and "filter effects," which assume that the tunneling process from the surface to the impurity through several insulating layers involves atomic states in several neighboring unit cells [25,26]. So far, these theories have been expressed entirely in terms of phenomenological effective hoppings in the Cu tight-binding model. First principles calculations for Zn in BSCCO in the normal state [27] provide some evidence in support of the filter picture, but until recently it was not possible to include both superconductivity and the various atomic wave functions extending into the barrier layers responsible for the filter. Nieminen *et al.* investigated the conductance spectrum in the BSCCO system using an analysis based on atomiclike wave functions [28], and showed that for the homogeneous system it could be decomposed in a series of tunneling paths, as postulated by the earlier crude proposals [25,26]. Using this approach one can explain, e.g., the spectral line shape at high bias voltage, but presently it is unclear how this approach applies to inhomogeneous problems.

The vast amount of STM data on cuprate surfaces have often been distilled using the quasiparticle interference (QPI), or Fourier transform STM spectroscopy technique, one of the most important modern techniques for unraveling the origin of high temperature superconductivity. This probe is sensitive to the wavelengths of Friedel oscillations caused by disorder, which then, in principle, contain information on the electronic structure of the pure system [29,30]. These wavelengths manifest themselves in the form of peaks at wave vectors $\mathbf{q}(\omega)$, which disperse with STM bias $V = \omega/e$ and represent scattering processes of high probability on the given Fermi surface. Many attempts have been made to calculate these patterns assuming simple tight-binding band structures, d-wave pairing, and methods ranging from single-impurity T matrix [31–37] to many-impurity solutions of the BdG equations [38]. While some similarities between the calculated patterns, the simplified so-called "octet model" [31], and experiment have been reported, there are always serious discrepancies, typically related not so much to the positions of peaks but rather their shapes and intensities.

In this Letter we revisit these classic unsolved problems using a new method called the BdG-Wannier (BdG + W) approach [39], which combines traditional solutions of the Bogoliubov–de Gennes equations with the microscopic Wannier functions obtained from downfolding density functional theory onto a low-energy effective tight-binding Hamiltonian. We show that the local density of states (LDOS) obtained from the continuum Green's function for a simple strong nonmagnetic impurity bound state in the BSSCO material with a d-wave superconducting gap displays excellent agreement with STM conductance maps (Fig. 1). We show furthermore that the QPI patterns obtained from such states, with generically weaker potentials to simulate out-of-plane native defects, agree much better with experiment than QPI maps obtained in previous theoretical calculations.

Model.—The starting point of our investigation is first principles calculations of a BSCCO surface [Fig. 2(a)] that yield a one band tight-binding lattice model for the noninteracting electrons $c_{\mathbf{R}\sigma}$ (with Hamiltonian $H_0 = \sum_{\mathbf{RR}',\sigma} t_{\mathbf{RR}'} c^\dagger_{\mathbf{R}\sigma} c_{\mathbf{R}'\sigma} - \mu_0 \sum_{\mathbf{R},\sigma} c^\dagger_{\mathbf{R}\sigma} c_{\mathbf{R}\sigma}$, where $t_{\mathbf{RR}'}$ are hopping elements between unit cells labeled $\mathbf{R}$ and $\mathbf{R}'$ and μ_0 is the chemical potential), and a Wannier basis $w_{\mathbf{R}}(\mathbf{r})$ with $\mathbf{r}$ describing the continuum position. The Wannier function, obtained from a projected Wannier function analysis [40], is primarily of Cu-$d_{x^2-y^2}$ character with in-plane oxygen p-orbital contributions, as can be seen in the isosurface plots for large values of the wave function, Fig. 2(b). However, it also contains contributions from atomic wave functions in neighboring elementary cells, in particular those from the apical oxygen atoms above the Cu plane, Fig. 2(c). These are the main source of the large lobes above the neighboring Cu atoms at the position of the STM tip above the Bi-O plane, Fig. 2(d). There is no weight, however, directly above the center Cu; see Fig. 2(d). This can be understood from the fact that the hybridization of the Cu-$d_{x^2-y^2}$ orbital with apical O-p and Bi-p orbitals in the same unit cell is forbidden by symmetry. In order to account for correlation effects at low energies, we use a mass renormalization factor of

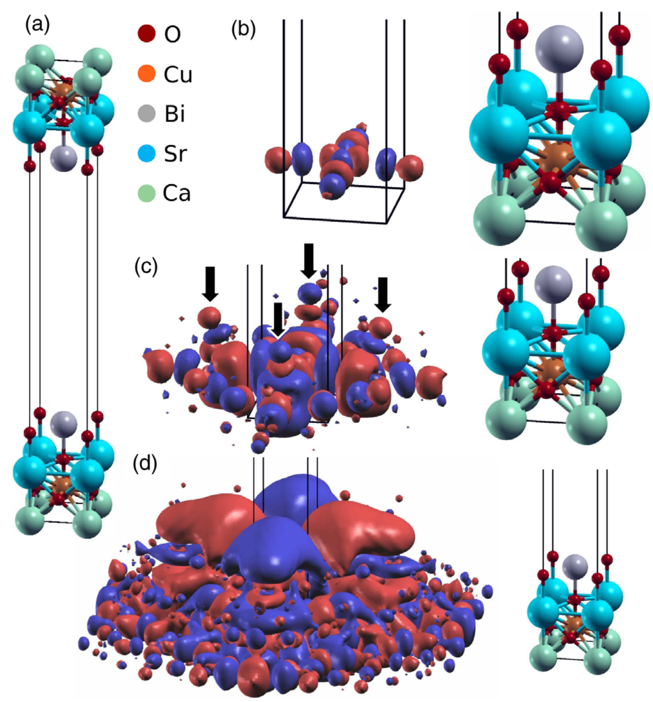

FIG. 2 (color online). (a) Elementary cell used in first principles calculation to obtain the electronic structure on the $Bi_2Sr_2CaCu_2O_8$ surface. Isosurface plots of the Cu-$d_{x^2-y^2}$ Wannier function at (b) 0.05, (c) 0.005, and (d) 0.0002 bohr$^{-3/2}$. Arrows indicate nearest-neighbor apical oxygen tails and red and blue indicate the sign of the Wannier function.

$1/Z = 3$ to scale down all hoppings such that the Fermi velocities approximately match the experimentally observed values [41] and fix the chemical potential to be at optimal doping, ($n = 0.85$).

Next, we solve the inhomogeneous mean field BdG equations for the full Hamiltonian of a superconductor in the presence of an impurity $H = H_0 + H_{\mathrm{BCS}} + H_{\mathrm{imp}}$, where the d-wave pairing interaction $\Gamma_{\mathbf{RR}'}$ (details in the Supplemental Material [42]) enters the calculation of the superconducting order parameter via $\Delta_{\mathbf{RR}'} = \Gamma_{\mathbf{RR}'}\langle c_{\mathbf{R}'\downarrow} c_{\mathbf{R}\uparrow}\rangle$ and gives rise to the second term $H_{\mathrm{BCS}} = -\sum_{\mathbf{R},\mathbf{R}'} \Delta_{\mathbf{RR}'} c^{\dagger}_{\mathbf{R}\uparrow} c^{\dagger}_{\mathbf{R}'\downarrow} + \mathrm{H.c.}$, while the third term is just a nonmagnetic impurity at lattice position $\mathbf{R}^*$, e.g., $H_{\mathrm{imp}} = \sum_\sigma V_{\mathrm{imp}} c^{\dagger}_{\mathbf{R}^*\sigma} c_{\mathbf{R}^*\sigma}$. From the BdG eigenvalues $E_{n\sigma}$ and eigenvectors $u_{n\sigma}$ and $v_{n\sigma}$ we can construct the usual retarded lattice Green's function

$$G_\sigma(\mathbf{R},\mathbf{R}';\omega) = \sum_n \left(\frac{u^{n\sigma}_{\mathbf{R}} u^{n\sigma *}_{\mathbf{R}'}}{\omega - E_{n\sigma} + i0^+} + \frac{v^{n-\sigma}_{\mathbf{R}} v^{n-\sigma *}_{\mathbf{R}'}}{\omega + E_{n-\sigma} + i0^+} \right), \tag{1}$$

and the corresponding continuum Green's function [39,51]

$$G_\sigma(\mathbf{r},\mathbf{r}';\omega) = \sum_{\mathbf{R},\mathbf{R}'} G_\sigma(\mathbf{R},\mathbf{R}';\omega) w_{\mathbf{R}}(\mathbf{r}) w^*_{\mathbf{R}'}(\mathbf{r}'), \tag{2}$$

by a simple basis transformation from the lattice operators $c_{\mathbf{R}\sigma}$ to the continuum operators $\psi_\sigma(\mathbf{r}) = \sum_{\mathbf{R}} c_{\mathbf{R}\sigma} w_{\mathbf{R}}(\mathbf{r})$, where the Wannier functions $w_{\mathbf{R}}(\mathbf{r})$ are the matrix elements. A similar transformation has been applied previously to understand neutron [52] and x-ray [53,54] spectra in the normal state. The continuum Green's functions can now be used to either calculate the LDOS $\rho(\mathbf{r},\omega) \equiv -(1/\pi)\mathrm{Im}G_\sigma(\mathbf{r},\mathbf{r};\omega)$ as measured in STS experiments [43] or obtain the QPI patterns by a Fourier transform. Before considering an impurity, we note that the basis transformation in Eq. (2) changes the spectral properties of the Greens function as it also contains terms that are nonlocal in the lattice description, e.g., $G_\sigma(\mathbf{R},\mathbf{R}';\omega)$ with $\mathbf{R} \neq \mathbf{R}'$. This has implications for the continuum LDOS $\rho(\mathbf{r},\omega)$, because the sign of $\mathrm{Im}G_\sigma(\mathbf{R},\mathbf{R}';\omega)$ is not fixed such that nonlocal contributions will lead to interference effects that can suppress or enhance the continuum LDOS at certain energies. These interference effects between Wannier functions are enhanced at the large distance from the surface where the STM tip is located and the Wannier functions are not confined by the lattice potential. To illustrate this, we show in Fig. 3(c) the spectral dependence of the lattice LDOS for a homogeneous calculation which shows the well-known V shape. Applying the basis transformation by summing only over terms with $\mathbf{R} = \mathbf{R}'$, this behavior is not altered by the continuum LDOS as seen from the overlaid black curve, while in the full expression the spectral dependence is qualitatively modified and displays a clear U-shaped LDOS at low energies. Experimentally

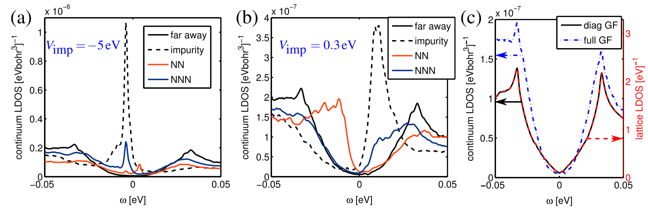

FIG. 3 (color online). (a) Continuum LDOS at 5 Å above the BiO surface in the superconducting state with a single Zn impurity modeled by an onsite -5 eV potential. Shown are positions directly above Cu atoms far from the impurity (black), at the impurity position (black, dashed), on the nearest neighbor position (red [light gray]), and on the next-nearest neighbor position (blue [dark gray]), calculated using 20×20 supercells with broadening of 1 meV and (b) for a weak impurity scatterer with $V_{\mathrm{imp}} = 0.3$ eV as used for the QPI analysis. In (c) we compare the spectral properties of the lattice density of states (red [light gray], dashed) with the continuum LDOS above a Cu atom calculated using the diagonal terms of the lattice Greens function $G_\sigma(\mathbf{R},\mathbf{R};\omega)$ only (black) and the full Green's function as given in Eq. (2) (blue [gray], dash dotted); all of them calculated for a homogeneous superconductor and scale adjusted such that two curves (black and red [light gray], dashed) exactly overlay.

obtained conductances reveal exactly such a U-shaped behavior in overdoped samples [55,56], and the transition from V-shaped LDOS to more U shaped has been observed with the same tip on samples with spatial inhomogeneous gaps [4,6,57]. We believe that these differences can be ascribed to the nonlocal contributions to Eq. (2).

Zn impurity.—A Zn impurity substituting for Cu in BSCCO produces a strong attractive potential which we simply model by an on-site potential of $V_{\mathrm{imp}} = -5$ eV, very similar to the value found in our first principles calculation (see Supplemental Material [42]). Calculating the LDOS, we find a sharp in-gap bound state peak around $\Omega_0 = -3.6$ meV, Fig. 3(a). The lattice LDOS from Eq. (1) shows a minimum at the impurity site and peaks at the NN sites [see Fig. 1(a) and Refs. [18,19]], precisely opposite from the experimental conductance map shown in Fig. 1(c). As pointed out in Refs. [25–28], the problem lies in the consideration of the Cu lattice sites far from the BiO surface. The correct quantity to study is the continuum LDOS $\rho(\mathbf{r},\Omega_0)$ at the height of the STM tip, which we assume to be at $z = 5$ Å above the BiO surface. The continuum LDOS obtained using Eq. (2) presented in Fig. 1(b) indeed shows a maximum on the impurity site, originating from adding the NN apical oxygen tails of the Cu Wannier functions adjacent to the Zn site, and longer range intensity tails that are rotated 45 degrees from the nodal directions of the d-wave gap, in excellent agreement with the experimental observation as taken from Ref. [8] [Fig. 1(c)]. We note a discrepancy on the 3rd site along the axis, where some of the reported experimental pattern are more intense than our theoretical result [8,15,16]. However, this peculiar feature seems not to be universal in experimental findings and might either be related to the local disorder environment on the surface of the crystal or the spatial supermodulation. Finer resolution resonances reported in Ref. [16] are also extremely similar to our calculations. While this is crudely the same agreement reported by filter-type theories [25,26], our calculation allows many further properties of the pattern to be recognized and provides a simple explanation of why they work. As in Ref. [27], the theory allows us to compare the LDOS in the CuO_2 plane to that detected at the surface, but now also includes the redistribution of spectral weight (into, e.g., coherence peaks and impurity bound states) caused by the opening of the superconducting gap.

QPI.—QPI patterns in BSCCO are generated by several different types of disorder, believed to consist primarily of out-of-plane defects such as interstitial oxygens or site switching of Bi and Sr atoms, whose potentials are not known microscopically. To account for these defects, we employ a weak potential scatterer on the Cu site with $V_{\mathrm{imp}} = 0.3$ eV and calculate the lattice LDOS and the continuum LDOS $\rho(\mathbf{r}, \omega)$, both of which show only redistribution of spectral weight close to the impurity; compare Fig. 3(b).

Calculating the Fourier transform of the conductances $g(\mathbf{r}, \omega) \propto \rho(\mathbf{r}, \omega)$ [44] in order to obtain the conductance maps $|g(\mathbf{q}, \omega)|$, one is immediately faced with the problem that the lattice LDOS only contains information on length scales $\geq a$. Thus, the maps only extend in $\mathbf{q}$ space to the first Brillouin zone $[-\pi/a \ldots \pi/a]$, while the Fourier transform of the continuum LDOS is not restricted in this way. The Fourier transformed maps have often been analyzed in terms of the octet model, which predicts a set of seven scattering vectors connecting hot spots at a given energy [31]. To compare to our result, we use the quasiparticle energies of our homogeneous superconductor to derive the expected QPI pattern. Figure 4 shows the calculated conductance maps $|g(\mathbf{q}, \omega)|$ at $\omega = 24$ meV for (a) the lattice model (BdG) and (b) the Wannier method (BdG + W), where the $\mathbf{q}$ vectors from the octet model have been marked by circles. In the BdG-only result, a few of the spots are reproduced, others are absent and, more importantly, the large $\mathbf{q}$ vectors are not accessible with the lattice model. In contrast, the map generated from the Wannier method shows a much better agreement with the octet model where all spots can be identified and no artificial spots appear. A full scan of energies to visually highlight the dispersive features of the spots can be seen as an animation in the Supplemental Material [42]. Note that it is mathematically not possible to obtain the BdG + W maps from the corresponding BdG maps since the former also contain nonlocal contributions, as explained in Ref. [39].

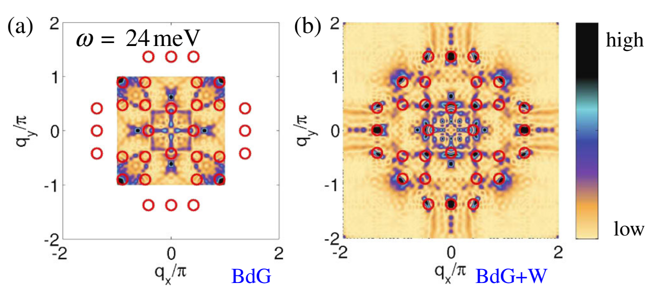

FIG. 4 (color online). Simulated QPI pattern from conductance maps: (a) Fourier transform of the lattice LDOS (BdG) and (b) Fourier transform of the continuum LDOS (BdG + W) at the same energy $\omega = 24$ meV. Impurity potential for the weak scatterer $V_{\mathrm{imp}} = 0.3$ eV. The red open symbols indicate the expected positions of the spots from the octet model.

In order to compare more closely to experiment, we follow Ref. [14] and simulate the maps of the differential conductance ratios $Z(\mathbf{q}, \omega)$ as well as the energy integrated maps $\Lambda(\mathbf{q})$ for both approaches; see definition in the Supplemental Material [42]. Figures 5(a)–5(c) show the Z maps of both methods side by side with an experimental result [17], demonstrating the improvement of our method (BdG + W) compared to the lattice BdG. Similarly, we compare maps of the integrated ratio $\Lambda(\mathbf{q})$: In Fig. 5(g) the experimental result is shown next to results from 3 different theoretical methods, (d) T-matrix simulation from Ref. [14], (e) lattice BdG, and (f) our BdG-Wannier method. While all three theoretical models obtain large weight around $(\pm\pi, \pm\pi)$, in agreement with experiment, only our Wannier method is capable of capturing

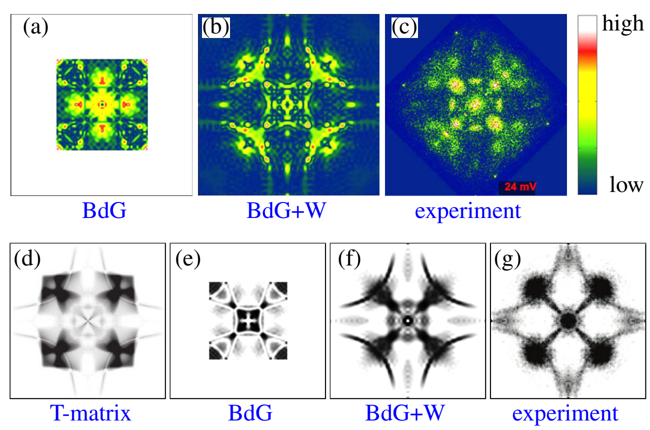

FIG. 5 (color online). (a) QPI Z map obtained from the Fourier transform of the real conventional space BdG patterns at $\omega = 24$ meV, (b) QPI Z map obtained from the Fourier transform of the continuous 3D LDOS $(x, y, z \approx 5\ \text{Å}; \omega)$ at $\omega = 24$ meV showing strong similarity to (c) the experimental results reproduced from Ref. [14] and rotated to match the orientation in (a) and (b). For the theoretical calculations a weak impurity scatterer of $V_{\mathrm{imp}} = 0.3$ eV was used. (d) T-matrix scattering interference simulation for $\Lambda(q)$ from Ref. [14]; (e) the same obtained from conventional BdG calculations; (f) Λ map obtained from the Fourier transform of the continuous 3D LDOS showing strong similarity to the experimental results (g) reproduced from Ref. [14]. All $\mathbf{q}$ maps are from $[-2\pi/a \ldots 2\pi/a]$.

simultaneously (1) the lines that extend from these large spots to the center, (2) the features along the axes between π and 2π, and (3) the arclike features that trace back the Fermi surface as in the analysis of Ref. [14].

Conclusions.—In this Letter we have illustrated the utility of calculating the continuum rather than the lattice Green's function to compare with STM data in inhomogeneous systems, using a first principles based Wannier function method. We have focused on the cuprate superconductor BSCCO, and calculated the Zn resonant LDOS as well as QPI patterns, showing in both cases dramatic improvement compared to experiment relative to traditional lattice-based BdG analysis. In the case of the Zn impurity, we have provided a first principles high-resolution theory of how electrons are transferred from nearest neighbor unit cells via apical oxygen atoms. In the case of the QPI patterns, the improved agreement is both with experiment and with the octet model. This shows that disagreements with the octet model in the past, primarily spurious arclike features and missing peaks, are due to the Fourier transform of the wrong electronic structure information: the lattice density of states in the CuO_2 plane rather than the continuous density of states at the STM tip position. It is clear that our results have implications that go beyond the simple dispersing QPI patterns of a disordered BCS d-wave superconductor. Any new theory of novel phenomena in the CuO_2 plane that seeks to compare with real space or QPI data should now be "dressed" with Wannier information, or risk misidentification of crucial scattering features.

The authors are grateful to J. Hoffman, Y. Wang, K. Fujita, and J. C. Davis for useful discussions. P. C., A. K., and P. J. H. were supported by DOE Grant No. DE-FG02-05ER46236, and T. B. as a Wigner Fellow at the Oak Ridge National Laboratory. B. M. A. and A. K. acknowledge support from Lundbeckfond Fellowship (Grant No. A9318). W. K. was supported by DOE-BES Grant No. DE-AC02-98CH10886. Work by T. B. was performed at the Center for Nanophase Materials Sciences, a DOE Office of Science user facility.

[1] O. Fischer, M. Kugler, I. Maggio-Aprile, C. Berthod, and C. Renner, Rev. Mod. Phys. **79**, 353 (2007).
[2] K. Fujita, A. R. Schmidt, E.-A. Kim, M. J. Lawler, D. Hai Lee, J. C. Davis, H. Eisaki, and S.-i. Uchida, J. Phys. Soc. Jpn. **81**, 011005 (2012).
[3] T. Cren, D. Roditchev, W. Sacks, and J. Klein, Europhys. Lett. **54**, 84 (2001).
[4] S. H. Pan, J. P. O'Neal, R. L. Badzey, C. Chamon, H. Ding, J. R. Engelbrecht, Z. Wang, H. Eisaki, S. Uchida, A. K. Gupta, K.-W. Ng, E. W. Hudson, K. M. Lang, and J. C. Davis, Nature (London) **413**, 282 (2001).
[5] C. Howald, P. Fournier, and A. Kapitulnik, Phys. Rev. B **64**, 100504 (2001).
[6] K. M. Lang, V. Madhavan, J. E. Hoffman, E. W. Hudson, H. Eisaki, S. Uchida, and J. C. Davis, Nature (London) **415**, 412 (2002).
[7] A. Yazdani, C. M. Howald, C. P. Lutz, A. Kapitulnik, and D. M. Eigler, Phys. Rev. Lett. **83**, 176 (1999).
[8] S. H. Pan, E. W. Hudson, K. M. Lang, H. Eisaki, S. Uchida, and J. C. Davis, Nature (London) **403**, 746 (2000).
[9] C. Howald, H. Eisaki, N. Kaneko, M. Greven, and A. Kapitulnik, Phys. Rev. B **67**, 014533 (2003).
[10] S. A. Kivelson, I. P. Bindloss, E. Fradkin, V. Oganesyan, J. M. Tranquada, A. Kapitulnik, and C. Howald, Rev. Mod. Phys. **75**, 1201 (2003).
[11] T. Hanaguri, C. Lupien, Y. Kohsaka, D.-H. Lee, M. Azuma, M. Takano, H. Takagi, and J. C. Davis, Nature (London) **430**, 1001 (2004).
[12] M. Vershinin, S. Misra, S. Ono, Y. Abe, Y. Ando, and A. Yazdani, Science **303**, 1995 (2004).
[13] Y. Kohsaka, C. Taylor, K. Fujita, A. Schmidt, C. Lupien, T. Hanaguri, M. Azuma, M. Takano, H. Eisaki, H. Takagi, S. Uchida, and J. C. Davis, Science **315**, 1380 (2007).
[14] K. Fujita, C. K. Kim, I. Lee, J. Lee, M. H. Hamidian, I. A. Firmo, S. Mukhopadhyay, H. Eisaki, S. Uchida, M. J. Lawler, E.-A. Kim, and J. C. Davis, Science **344**, 612 (2014).
[15] T. Machida, T. Kato, H. Nakamura, M. Fujimoto, T. Mochiku, S. Ooi, A. D. Thakur, H. Sakata, and K. Hirata, Phys. Rev. B **84**, 064501 (2011).
[16] M. H. Hamidian, I. A. Firmo, K. Fujita, S. Mukhopadhyay, J. W. Orenstein, H. Eisaki, S. Uchida, M. J. Lawler, E.-A. Kim, and J. C. Davis, New J. Phys. **14**, 053017 (2012).
[17] The experimental pattern shows a C_2 symmetry that is attributed to the structural supermodulation, which is not considered in our work.
[18] A. V. Balatsky, I. Vekhter, and J.-X. Zhu, Rev. Mod. Phys. **78**, 373 (2006).
[19] H. Alloul, J. Bobroff, M. Gabay, and P. J. Hirschfeld, Rev. Mod. Phys. **81**, 45 (2009).
[20] A. Polkovnikov, S. Sachdev, and M. Vojta, Phys. Rev. Lett. **86**, 296 (2001).
[21] M. E. Flatté, Phys. Rev. B **61**, R14920 (2000).
[22] J.-M. Tang and M. E. Flatté, Phys. Rev. B **66**, 060504 (2002).
[23] J.-M. Tang and M. E. Flatté, Phys. Rev. B **70**, 140510 (2004).
[24] B. M. Andersen, A. Melikyan, T. S. Nunner, and P. J. Hirschfeld, Phys. Rev. Lett. **96**, 097004 (2006).
[25] J.-X. Zhu, C. S. Ting, and C.-R. Hu, Phys. Rev. B **62**, 6027 (2000).
[26] I. Martin, A. V. Balatsky, and J. Zaanen, Phys. Rev. Lett. **88**, 097003 (2002).
[27] L.-L. Wang, P. J. Hirschfeld, and H.-P. Cheng, Phys. Rev. B **72**, 224516 (2005).
[28] J. Nieminen, I. Suominen, R. S. Markiewicz, H. Lin, and A. Bansil, Phys. Rev. B **80**, 134509 (2009).
[29] P. T. Sprunger, L. Petersen, E. W. Plummer, E. Lgsgaard, and F. Besenbacher, Science **275**, 1764 (1997).
[30] J. E. Hoffman, K. McElroy, D.-H. Lee, K. M. Lang, H. Eisaki, S. Uchida, and J. C. Davis, Science **297**, 1148 (2002).
[31] Q.-H. Wang and D.-H. Lee, Phys. Rev. B **67**, 020511 (2003).
[32] L. Capriotti, D. J. Scalapino, and R. D. Sedgewick, Phys. Rev. B **68**, 014508 (2003).

[33] T. Pereg-Barnea and M. Franz, Phys. Rev. B **68**, 180506 (2003).
[34] D. Zhang and C. S. Ting, Phys. Rev. B **67**, 100506 (2003).
[35] B. M. Andersen and P. Hedegård, Phys. Rev. B **67**, 172505 (2003).
[36] T. S. Nunner, W. Chen, B. M. Andersen, A. Melikyan, and P. J. Hirschfeld, Phys. Rev. B **73**, 104511 (2006).
[37] E. A. Nowadnick, B. Moritz, and T. P. Devereaux, Phys. Rev. B **86**, 134509 (2012).
[38] L. Zhu, W. A. Atkinson, and P. J. Hirschfeld, Phys. Rev. B **69**, 060503 (2004).
[39] P. Choubey, T. Berlijn, A. Kreisel, C. Cao, and P. J. Hirschfeld, Phys. Rev. B **90**, 134520 (2014).
[40] W. Ku, H. Rosner, W. E. Pickett, and R. T. Scalettar, Phys. Rev. Lett. **89**, 167204 (2002).
[41] A. Damascelli, Z. Hussain, and Z.-X. Shen, Rev. Mod. Phys. **75**, 473 (2003).
[42] See Supplemental Material at http://link.aps.org/supplemental/10.1103/PhysRevLett.114.217002 for technical details on the calculation of the Wannier functions, the Zn impurity potential and the tight binding model from first principles, a summary of the calculational steps to obtain the conductance maps and QPI pattern as well as a set of results for different choices of parameters, and which includes Refs. [14,31,40,43–50].
[43] J. Tersoff and D. R. Hamann, Phys. Rev. B **31**, 805 (1985).
[44] J. E. Hoffman, Rep. Prog. Phys. **74**, 124513 (2011).
[45] M. S. Hybertsen and L. F. Mattheiss, Phys. Rev. Lett. **60**, 1661 (1988).
[46] K. Schwarz, P. Blaha, and G. Madsen, Comput. Phys. Commun. **147**, 71 (2002).
[47] V. I. Anisimov, D. E. Kondakov, A. V. Kozhevnikov, I. A. Nekrasov, Z. V. Pchelkina, J. W. Allen, S.-K. Mo, H.-D. Kim, P. Metcalf, S. Suga, A. Sekiyama, G. Keller, I. Leonov, X. Ren, and D. Vollhardt, Phys. Rev. B **71**, 125119 (2005).
[48] E. W. Hudson, K. M. Lang, V. Madhavan, S. H. Pan, H. Eisaki, S. Uchida, and J. C. Davis, Nature (London) **411**, 920 (2001).
[49] Y. He, Y. Yin, M. Zech, A. Soumyanarayanan, M. M. Yee, T. Williams, M. C. Boyer, K. Chatterjee, W. D. Wise, I. Zeljkovic, T. Kondo, T. Takeuchi, H. Ikuta, P. Mistark, R. S. Markiewicz, A. Bansil, S. Sachdev, E. W. Hudson, and J. E. Hoffman, Science **344**, 608 (2014).
[50] N. Marzari and D. Vanderbilt, Phys. Rev. B **56**, 12847 (1997).
[51] L. Dell'Anna, J. Lorenzana, M. Capone, C. Castellani, and M. Grilli, Phys. Rev. B **71**, 064518 (2005).
[52] A. C. Walters, T. G. Perring, J.-S. Caux, A. T. Savici, G. D. Gu, C.-C. Lee, W. Ku, and I. A. Zaliznyak, Nat. Phys. **5**, 867 (2009).
[53] B. C. Larson, W. Ku, J. Z. Tischler, C.-C. Lee, O. D. Restrepo, A. G. Eguiluz, P. Zschack, and K. D. Finkelstein, Phys. Rev. Lett. **99**, 026401 (2007).
[54] P. Abbamonte, T. Graber, J. P. Reed, S. Smadici, C.-L. Yeh, A. Shukla, J.-P. Rueff, and W. Ku, Proc. Natl. Acad. Sci. U.S.A. **105**, 12159 (2008).
[55] Y. Kohsaka, C. Taylor, P. Wahl, A. Schmidt, J. Lee, K. Fujita, J. W. Alldredge, K. McElroy, J. Lee, H. Eisaki, S. Uchida, D.-H. Lee, and J. C. Davis, Nature (London) **454**, 1072 (2008).
[56] K. McElroy, D.-H. Lee, J. E. Hoffman, K. M. Lang, J. Lee, E. W. Hudson, H. Eisaki, S. Uchida, and J. C. Davis, Phys. Rev. Lett. **94**, 197005 (2005).
[57] J. W. Alldredge, J. Lee, K. McElroy, M. Wang, K. Fujita, Y. Kohsaka, C. Taylor, H. Eisaki, S. Uchida, P. J. Hirschfeld, and J. C. Davis, Nat. Phys. **4**, 319 (2008).